ELSEVIER

Earth and Planetary Science Letters 183 (2000) 215–229

EPSL

www.elsevier.com/locate/epsl

Predicting paleoelevation of Tibet and the Himalaya from $\delta^{18}O$ vs. altitude gradients in meteoric water across the Nepal Himalaya

Carmala N. Garzione [a,*], Jay Quade [b], Peter G. DeCelles [b], Nathan B. English [b]

[a] Department of Earth and Environmental Sciences, University of Rochester, Rochester, NY 14627, USA
[b] Department of Geosciences, University of Arizona, Tucson, AZ 85721, USA

Received 26 May 2000; received in revised form 3 August 2000; accepted 8 September 2000

Abstract

The $\delta^{18}O$ value of meteoric water varies with elevation, providing a means to reconstruct paleoelevation if the $\delta^{18}O$ values of paleowater are known. In this study, we determined the $\delta^{18}O$ values of water ($\delta^{18}O_{mw}$) from small tributaries along the Seti River and Kali Gandaki in the Nepal Himalaya. We found that $\delta^{18}O_{mw}$ values decrease with increasing altitude for both transects. $\delta^{18}O_{mw}$ vs. altitude along the Kali Gandaki in west-central Nepal fit a second order polynomial curve, consistent with increasing depletion of ^{18}O with increasing elevation, as predicted by a Rayleigh-type fractionation process. This modern $\delta^{18}O_{mw}$ vs. altitude relationship can be used to constrain paleoelevation from the $\delta^{18}O$ values of Miocene–Pliocene carbonate ($\delta^{18}O_c$) deposited in the Thakkhola graben in the southern Tibetan Plateau. Paleoelevations of 3800 ± 480 m to 5900 ± 350 are predicted for the older Tetang Formation and 4500 ± 430 m to 6300 ± 330 m for the younger Thakkhola Formation. These paleoelevation estimates suggest that by ~ 11 Ma the southern Tibetan Plateau was at a similar elevation to modern.

Keywords: O-18/O-16; altitude; streams; surface water; Nepal; Himalayas

1. Introduction

Altitude across the topographic front of the Himalaya increases from approximately 200 m in the Gangetic foreland basin to 8000+ m at the tallest peaks. North of the high Himalaya, the Tibetan Plateau has an average elevation > 5000 m [1]. Understanding when and how the Himalaya and Tibet attained their current elevations is important for evaluating the effects of high topography on south Asian ecology, regional and global climate, and ocean chemistry [2–8].

Previous work has demonstrated that oxygen isotopes of lacustrine and paleosol carbonate can be used as a gauge of paleoelevation (e.g., [9–11]) because they are partially determined by the $\delta^{18}O$ value of meteoric water ($\delta^{18}O_{mw}$), which is largely dependent on elevation. As a vapor mass rises in elevation, it expands and cools, caus-

* Corresponding author. Tel.: +1-716-273-4572; Fax: +1-716-244-5689; E-mail: garzione@earth.rochester.edu

0012-821X/00/$ – see front matter
PII: S0012-821X(00)00252-1

ing rainout, and producing lower $\delta^{18}O_{mw}$ values at progressively higher elevation. Modern world-wide gradients of $\delta^{18}O_{mw}$ (Vienna Standard Mean Ocean Water (VSMOW)) vs. altitude fall in a range from -0.1‰ to -1.1‰/100 m, with a global mean gradient of -0.26‰/100 m [12]. Oxygen isotopic partitioning trends generally fit Rayleigh-type fractionation models [13,14], complicated by processes such as evapotranspiration and vertical mixing in a cloud system (e.g., [15,16]).

The $\delta^{18}O$ values of carbonate ($\delta^{18}O_c$) from Tibet and the Himalaya are potentially useful for understanding the development of high elevation on the plateau. Carbonate from the Thakkhola graben on the southern Tibetan Plateau yield $\delta^{18}O_c$ (Vienna Peedee belemnite (VPDB)) values between -16‰ and -23‰, consistent with formation at very high elevation [11]. However, paleoelevation reconstructions rely on knowledge of the $\delta^{18}O_{mw}$ vs. altitude relationship, which is sparsely documented in the Himalaya. Two studies of river waters in India report linear gradients of $\delta^{18}O_{mw}$ vs. altitude of -0.19‰/100 for the headwaters of the Ganges between 300 and 3000 m [17] and -0.14‰/100 m for surface waters in the Gaula river catchment in Kumaun, India between 915 and 2150 m [18]. Another study of thermal waters determined a range of 0.2 to 0.3‰/100 [19]. In this study, we measured $\delta^{18}O$ values of small streams along two transects across the Himalayan orogen in Nepal, from the foothills to the Tibetan Plateau (Fig. 1). Our objective is to determine an empirical relationship for the modern $\delta^{18}O_{mw}$ vs. altitude gradient and to compare it to the paleocarbonate record from the Tibetan Plateau to understand the elevation history of the plateau. We chose these transects because they provide a N–S profile across the Himalaya and southern Tibet, allowing sampling along elevation gradients across the approximate trajectory of rainfall as it moves over the Himalayan range. Streams more closely represent meteoric water compositions of average annual rainfall if sampled during the dry season when groundwater dominates the stream water budget, because groundwater contains a mixture of rainfall throughout the annual cycle [20,21]. Although maintaining rain collection stations across the Himalayan fold-thrust belt would provide better estimates of average meteoric water composition, sampling stream water is much more feasible.

2. Geology

2.1. Himalayan fold–thrust belt and southern Tibetan Plateau

The Himalayan fold–thrust belt in Nepal consists of four regional lithotectonic packages separated by major fault zones. The northern boundary of the fold–thrust belt is the Indus suture zone (Fig. 1A), which sutures the Eurasian and Indian plates [22,23]. South of the suture zone lies the Tibetan Himalaya, which consists of Cambrian–Eocene sedimentary rocks of the Tethyan Series that are incorporated into numerous south-verging thrust sheets [23–25]. The southern boundary of the Tibetan Himalaya is the South Tibetan detachment system, a system of north-dipping, normal-sense detachment faults that juxtapose the Tethyan Series against Greater Himalayan rocks [24,26]. Greater Himalayan rocks consist of late Proterozoic to early Paleozoic [27,28] paragneisses, orthogneisses, and schists that were metamorphosed to amphibolite grade during the Cenozoic orogenic event. These rocks have been thrust southward along the Main Central thrust system upon lower to upper greenschist grade metasedimentary rocks of the Lesser Himalayan zone [29–31]. Lesser Himalayan rocks, which consist of early to middle Proterozoic passive margin sequences have been thrust southward along the Main Boundary thrust system. The frontal, Subhimalayan zone of the fold–thrust belt comprises an imbricate thrust system in Neogene foreland basin deposits of the Siwalik Group.

The kinematic history of the Himalayan fold–thrust belt followed a generally southward progression of emplacement of the major thrust systems [31–33]. Tibetan thrusts were active mainly during Eocene and Oligocene time [23,25], and produced regional Barrovian metamorphism of underlying Greater Himalayan rocks [34]. Thermochronologic data from Greater Himalayan

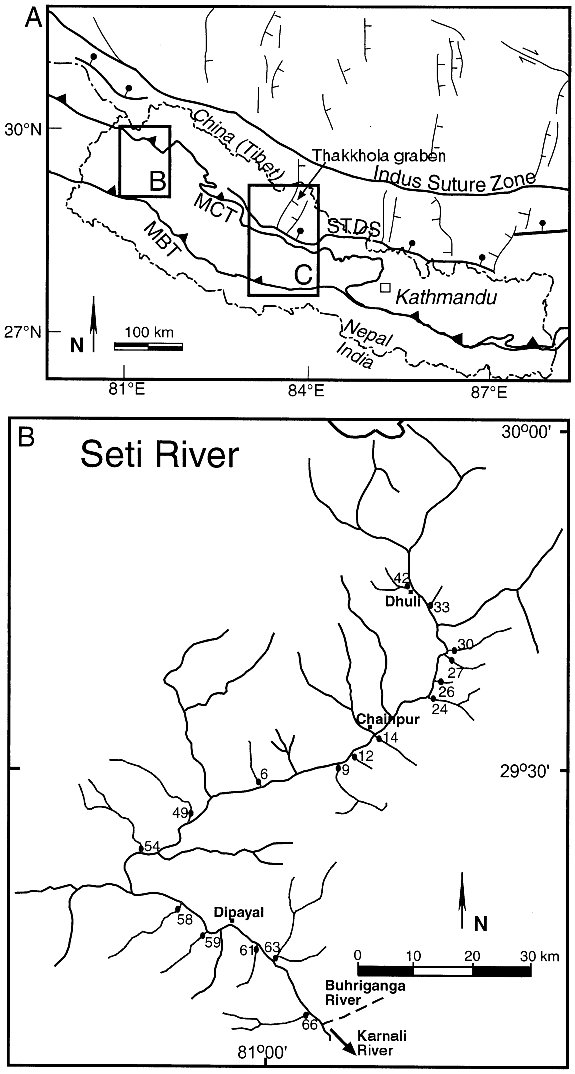

Fig. 1. (A) General tectonic map of the southern Tibetan Plateau and Nepal Himalaya. Hachures are north-south striking normal faults. Lines with ball and stick ornaments are South Tibetan Detachment system (STDS). Barbed lines are Main Central thrust (MCT) and Main Boundary thrust (MBT). Thakkhola graben is shown. Boxes show locations of study areas detailed in 1B and 1C. (B) Map of the Seti River showing tributary sample localities. (C) Map of the Kali Gandaki showing tributary sample localities. Small sampled tributaries are shown as medium gray and large tributaries sampled in the Thakkhola graben are shown as light gray.

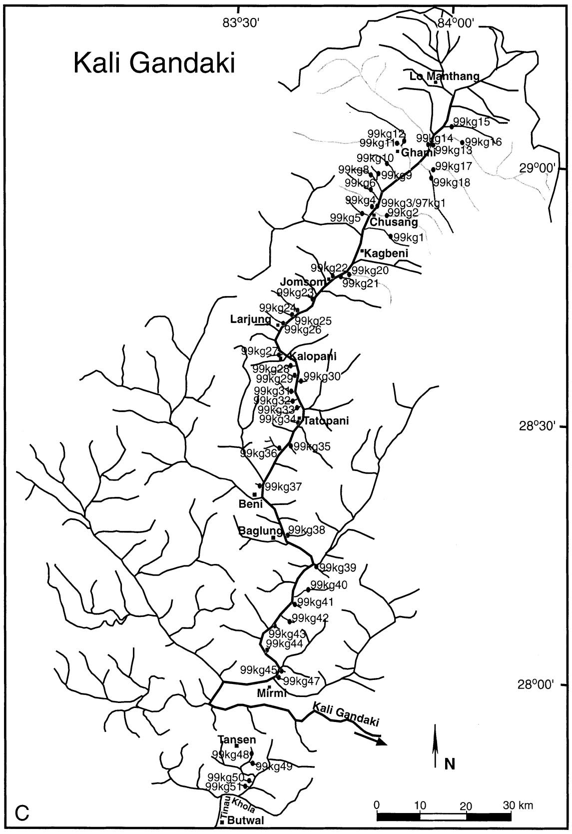

Fig. 1 (*continued*).

rocks suggest rapid cooling during late Oligocene–early Miocene time, presumably during emplacement of the Main Central thrust system (e.g., [35,36]). At about the same time, the South Tibetan detachment system became active (e.g., [36,37]). Since middle Miocene time the deformation front has migrated southward into the Lesser Himalayan and Subhimalayan zones [38,39]. Estimates of regional shortening rates in the Himalayan fold–thrust belt in Nepal during the Neogene [39–41] and the Paleogene [33] are similar to modern rates of shortening determined by space geodetic measurements [42]. Observations that (1) crustal thickening sufficient to drive Barrovian metamorphism in Greater Himalayan rocks was underway during Eocene and Oligocene time and (2) the Himalayan foreland basin has been filled above sea level since at least late Oligocene time

Table 1
Oxygen isotopic data and elevation information for sampled tributaries along the Seti River and Kali Gandaki

Sample name	Tributary/river	Sampling elevation (m)	Tributary elevation range (m)	$\delta^{18}O$(VSMOW) (‰)	δD(VSMOW) (‰)
Seti River					
42	Gadpai Gad	2350	2740	−10.4	
				−10.5	
33	Ramus Khola	2040	3110	−10.5	
30	Panai Gad	1770	2200	−10.2	
27	Lisni Khola	1710	1400	−9.7	
26	Unnamed	1590	900	−9.1	
24	Talkoti Gad	1460	1500	−8.4	
14	Dungri Khola	1310	900	−9.7	
12	Dil Gad	1220	1300	−9.5	
				−9.5	
9	Jidear Gad	1130	2050	−9.3	
6	Juili Gad	910	900	−8.8	
49	Nayagari Khola	820	1450	−7.7	
54	Dhung Gad	720	1550	−7.8	
58	Rori Gad	610	900	−7.4	
59	Kali Gad	570	1000	−7.7	
61	Unai Gad	530	1000	−7.7	
63	Gandi Gad	490	1050	−7.7	
66	Bheri Khola	430	1050	−7.2	
69	Chairo Khola	370	1450	−6.8	
Kali Gandaki					
99kg9	Unnamed	3900	1850	−17.5	−128
				−17.4	
99kg8	Unnamed	3800	1450	−18.3	
99kg10	Giling Khola	3750	250	−17.4	
99kg11	Qumona Khola	3700	2200	−20.5	
99kg12	Unnamed	13700	1550	−19.3	−143
99kg6	Samar Khola	3670	1800	−17.6	−128
99kg16	Ghechang Khola	3550	2450	−19.8	
99kg15	Puyon Khola	3500	2000	−18.5	
99kg1	Ghidiya Khola	3450	1800	−17.7	−113
99kg18	Yak Khola	3410	2350	−18.8	−139
99kg13	*Kali Gandaki*	3300	*	−19.5	
99kg14	Tsarang Khola	3300	2500	−21.2	
99kg17	Tange Khola	3280	2450	−19.1	
99kg5	Unnamed	3250	2000	−17.5	
97kg1	*Kali Gandaki*	3000	*	−18.2	
99kg3	*Kali Gandaki*	3000	*	−19.5	
99kg2	Narsing Khola	2960	2750	−18.8	
99kg4	Chele Khola	2960	2750	−17.5	
99kg20	Panda Khola	2800	2500	−16.5	
99kg22	Unnamed	2750	1700	−15.7	−115
99kg21	Unnamed	2700	600	−13.7	
99kg23	Unnamed	2600	1000	−11.2	−76
99kg24	Yamkin Khola	2500	1400	−13.4	−92
99kg25	Unnamed	2500	1400	−12.8	
99kg26	Largung Khola	2440	1800	−12.2	−84
99kg27	Unnamed	2300	1800	−13.0	
99kg28	Kaiku Khola	2000	2300	−11.9	−82
99kg29	Ghasa Khola	1850	1400	−11.2	
99kg30	Unnamed	1800	1600	−12.0	−84

Table 1 (*continued*)

Sample name	Tributary/river	Sampling elevation (m)	Tributary elevation range (m)	$\delta^{18}O$(VSMOW) (‰)	δD(VSMOW) (‰)
99kg31	Rupse Khola	1700	2300	−11.4	
99kg32	Dana Khola	1400	1550	−10.0	−68
99kg33	Bhalu Khola	1350	2250	−10.6	
				−10.7	
99kg34	Unnamed	1240	1060	−9.6	−67
99kg35	Thado Khola	1140	1540	−10.7	
99kg36	Beg Khola	1040	1840	−9.8	−68
99kg37	Unnamed	870	210	−9.5	
99kg48	Hulandi Khola	855	500	−9.0	
99kg49	Unnamed	820	330	−9.2	−67
99kg40	Dundure Khola	800	320	−9.6	−68
99kg42	Buchchha Khola	790	1210	−9.4	−67
99kg38	Damuwa Khola	760	1140	−9.6	−70
99kg41	Luha Khola	720	780	−9.8	
99kg43	Phoksin Khola	720	1280	−9.7	
99kg45	Unnamed	720	180	−8.7	
99kg39	Malyandi Khola	680	920	−9.3	
99kg50	Unnamed	660	160	−8.7	
99kg44	Unnamed	620	160	−8.2	
99kg47	Unnamed	620	660	−8.8	−62
99kg51	Unnamed	480	220	−8.1	−60

Data for each location appear in order from highest to lowest sampling elevation. Tributary elevation range (m) is the number of meters of elevation above the sampling elevation over which the tributary flows. Seti River tributary data also appear in [52].

[43,33], suggest that the Himalayan fold–thrust belt attained high elevations by Oligocene time.

2.2. Thakkhola graben

Thakkhola graben is located in north-central Nepal, on the southern edge of the Tibetan Plateau, between the South Tibetan Detachment system and the Indus Suture zone (Fig. 1A). The Kali Gandaki drains the southern Tibetan Plateau in this region, flowing southward along the axis of the graben and through the fold–thrust belt to the Himalayan foreland basin. The Thakkhola graben is bound by faults to the east and west, with Tethyan Series rocks in its footwalls [44]. Basin-fill deposits are exposed between 3000 and 4200 m in the basin. Two depositional sequences, separated by an angular unconformity, make up the basin fill [45,46]. The older Tetang Formation (up to 230 m thick) crops out in the southeastern part of the basin and consists of fluvial deposits that grade into lacustrine deposits toward the top of the section. Magnetostratigraphic data suggest an age of $\sim$11 to 10.5 Ma for the onset of deposition of the Tetang Formation [11]. The overlying Thakkhola Formation (up to 1000 m thick) is exposed throughout the basin and consists of alluvial fan deposits along the western basin-bounding fault, and fluvial and lacustrine deposits in the central and eastern parts of the basin. The presence of C_4 vegetation reconstructed from the soil carbonate record of the Thakkhola Formation constrains its age to <7 Ma [11]. Paleocurrent indicators suggest southward axial drainage since the beginning of Thakkhola Formation deposition [46]. More recently, the Kali Gandaki has incised through at least 1000 m of basin fill, into Cretaceous Tethyan Series rocks. Several cycles of Pleistocene deposition within the incised valley indicate that the basin has experienced multiple phases of Pleistocene damming and incision [45,47,48]

3. Hydrology and meteorology of the Himalaya and southern Tibet

Most rainfall in the Himalaya and southern

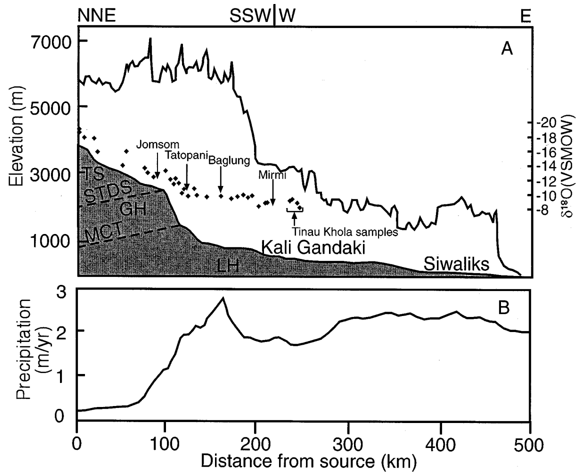

Fig. 2. Elevation profiles, tributary $\delta^{18}O$ values, and rainfall profile across the Kali Gandaki drainage plotted against distance from source of the Kali Gandaki. (A) Elevation profile of the Kali Gandaki is shown as shaded region and average crest elevation is shown as black line (from [51]. Tributary $\delta^{18}O$ values are plotted at location of sampling along the Kali Gandaki. Principle bedrock provinces: Tethyan Series (TS), Greater Himalaya (GH), Lesser Himalaya (LH), and fault systems: South Tibetan Detachment System (STDS), Main Central Thrust (MCT). (B) Average annual precipitation across the Kali Gandaki drainage profile (from [51]).

Tibet occurs during the summer monsoon. Rain stations at New Delhi, Kathmandu, and Lhasa record more than 85% of annual precipitation from May to September, during the summer monsoon [49]. The monthly average discharge of major rivers that flow southward out of the fold–thrust belt increases by an order of magnitude during the summer monsoon [50]. Precipitation varies greatly between the Himalaya and Tibet as a result of the high Himalayan rainshadow (Fig. 2B). South of the high Himalaya, across the central Nepal fold–thrust belt, the mean annual rainfall is between ~ 100 and 500 cm/yr, whereas north of the high Himalaya, in the Thakkhola graben, rainfall is < 40 cm/yr [50].

The Kali Gandaki and Seti River flow southward through the Himalayan fold–thrust belt, joining the Ganges River system in the foreland. These rivers drain the southern edge of the Tibetan Plateau, north of the South Tibetan Detachment system and south of the Indus Suture zone. A drainage profile along the Kali Gandaki [51] has a large nick point associated with the Main Central thrust and high Himalaya (Fig. 2A). To a large extent, this steep stream gradient is a result of the more resistant rock types in the Greater Himalaya.

4. Sampling and analytical methods

Eighteen tributaries to the Seti River (Fig. 1B) and 46 tributaries to the Kali Gandaki (Fig. 1C) were sampled during foot traverses in March–April 1998 and late September–October 1999, respectively. We collected during the dry season in order to sample base-level flows, which give a closer approximation of mean annual precipitation [20,21]. Generally, we sampled tributaries that flow perennially over an elevation range of < 2000 m (henceforth termed 'small tributaries') for the $\delta^{18}O_{mw}$ vs. altitude transect. Tributaries with perennial flow over an elevation range > 2000 m we term 'large tributaries.' We sampled both large and small tributaries north of Jomsom along the Kali Gandaki traverse, in order to characterize the complete range of modern $\delta^{18}O_{mw}$ values in the Thakkhola graben.

In the field, water samples were sealed in 15 ml polyethylene bottles. Samples were transported and stored in darkness and refrigerated during storage prior to analysis. Elevations were determined with a Garmin Model 45 GPS unit and cross-checked with 1:25,000 to 1:125,000 topographic maps for accuracy along the Kali Gandaki. Elevations were determined from 1:63 360 scale maps along the Seti River.

For oxygen isotope analysis, 5 ml of water was equilibrated with CO_2 at 16°C for 8 h. Gasses were analyzed on a Finnegan MAT Delta gas-ratio mass spectrometer. Precision was ± 0.07‰ for $\delta^{18}O$ of five replicate pairs of water. Twenty-seven internal standards run during the time of analysis yielded standard deviations ± 0.05. On the basis of these data, the overall external precision was $< \pm 0.1$‰ (1σ). All water results are presented in VSMOW.

5. Results

5.1. Seti transect

Tributaries to the Seti River were sampled between 365 and 2350 m (Table 1 and Fig. 3). $\delta^{18}O_{mw}$ plotted against altitude yields a best-fit line with a slope of −0.18‰/100 m, with a regression coefficient (R^2) of 0.85 (n = 18). We sampled from Jiuli Gad (6) north to Gadpai Gad (42), and then from Nayagari Khola (49) south to Chairo Khola (69 – just off of map) (Fig. 1B). The first samples (6, 9, 12, and 14) were collected prior to several large rainfall events. The first rainfall event lasted ~12 h and raised the water level in the Seti River substantially. After rainfall 1, the first tributary sampled upstream (24) had a $\delta^{18}O$ value 1.3‰ higher than the last downstream tributary (14), sampled just before the storm (Fig. 3). This suggests that rainfall run-off had higher $\delta^{18}O$ values than base-level flow, and is consistent with measurements of higher $\delta^{18}O$ values for winter/spring rainfall compared to summer monsoon rainfall in the Himalaya [53]. Over several days of water sampling subsequent to rainfall 1, $\delta^{18}O_{mw}$ values declined as run-off decreased. Rainfall 2, which lasted ~8 h, also caused an increase in tributary $\delta^{18}O$ values (Fig. 3). During collection of the final set of samples below Jiuli Gad (49–69), no rainfall events occurred. The addition of rainfall with high $\delta^{18}O$ values to upstream tributaries (24–42) decreases the gradient of $\delta^{18}O$ vs. altitude estimated for far-western Nepal. Excluding these data, a linear regression through tributaries from 365 to 1310 m yields a best-fit line with a slope of −0.29‰/100 m and R^2 = 0.92 (n = 12) (Fig. 3). At the 95% confidence limit, the slope varies between −0.23‰/100 m and −0.35‰/100 m and the y-intercept between −5.4‰ and −6.4‰.

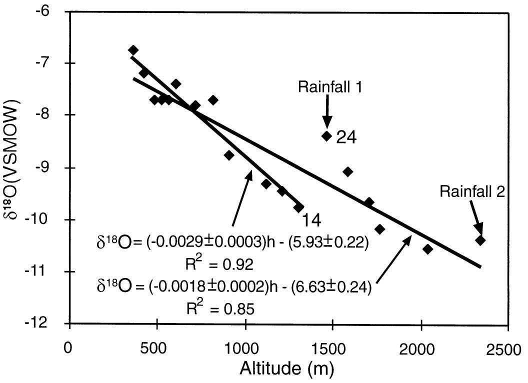

Fig. 3. $\delta^{18}O$ vs. altitude for tributaries sampled along the Seti River in far-western Nepal during March/April 1998. Rainfalls 1 and 2 show the first samples collected after rainfall events. The positive shift in tributary $\delta^{18}O$ values subsequent to rainfall events indicates that spring rainfall is relatively more positive than base-level flow. See text for discussion of regression lines.

5.2. Kali Gandaki transect

Tributaries to the Kali Gandaki and Tinau Khola (just south of the eastward bend in the Kali Gandaki) were sampled between elevations of 480 and 3900 m. (Fig. 1C). We sampled both large and small tributaries north of Kagbeni, in the Thakkhola graben, to characterize the full range of $\delta^{18}O$ values of river water. Tributaries of the Thakkhola graben, sampled between 2960 and 3900 m, yield $\delta^{18}O$ values ranging from −15.7‰ to −21.2‰ (Table 1 and Fig. 1C). Small tributaries have higher $\delta^{18}O$ values (−15.7‰ to −19.3‰) than large tributaries sampled at the same elevations (−16.5‰ and −21.2‰), because the larger tributaries have catchment areas that reach higher elevations and therefore carry a greater proportion of high elevation precipitation (Fig. 4). Large tributaries increase the scatter in the data, producing a spurious $\delta^{18}O_{mw}$ vs. altitude gradient and are therefore excluded from the $\delta^{18}O_{mw}$ vs. altitude regression.

We determined δD values from 20 water samples, representing the full range of elevations, so that we could evaluate the possibility of kinetic evaporation effects as moisture moves northward beyond the high Himalaya onto the Tibetan Plateau. A linear regression through the data produces a local meteoric water line of:

$$\delta D = (7.59 \pm 0.14)\delta^{18}O + (5.67 \pm 1.9) \quad (1)$$

yielding an R^2 = 0.99. The excellent line-fit to a slope of ~8 indicates that there are no significant

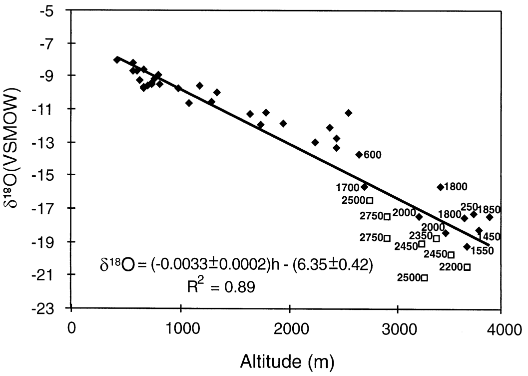

Fig. 4. $\delta^{18}O$ vs. altitude for all tributaries sampled along the Kali Gandaki and Tinau Khola in west-central Nepal during September/October 1999. Large tributaries (>2000 m elevation range) north of Jomsom are shown as open squares and all other tributaries are shown as filled diamonds. Labels for tributaries north of Jomsom indicate the tributary elevation range. More negative $\delta^{18}O$ values of large tributaries indicate they carry a greater proportion of high-elevation precipitation.

kinetic evaporation effects during rainfall in the arid region north of the high Himalaya.

Tributary $\delta^{18}O$ values plotted next to the Kali Gandaki stream profile indicate there is a strong correlation between oxygen isotopic fractionation and local sampling elevation (Fig. 2A). Where the Kali Gandaki stream gradient is steeper, $\delta^{18}O_{mw}$ values decrease more rapidly. The correlation between the Kali Gandaki gradient and tributary $\delta^{18}O$ values suggests that elevation changes are the dominant cause of rainout and that the $\delta^{18}O$ value of small tributaries represents rainfall at local elevations, rather than at high elevations on the surrounding peaks (black line, Fig. 2A). Even in the arid region north of the high peaks, the decrease in tributary $\delta^{18}O$ values reflects the Kali Gandaki stream gradient, which suggests that the effects of evaporation are negligible.

A plot of $\delta^{18}O$ values of tributaries vs. altitude yields a best-fit line with a slope of -0.29 ‰/100 m and $R^2 = 0.93$ ($n = 38$) (Fig. 5). One data point (99kg23) falls significantly above the line. This data point fits the local meteoric water line, which indicates that disequilibrium evaporation processes are not responsible for the high value. Possible causes of the higher $\delta^{18}O$ value are that the stream water has undergone equilibrium evaporation or the stream carries a greater proportion of winter rainfall than other sampled tributaries. A second order polynomial provides a better fit to the data ($R^2 = 0.96$) (Fig. 5), yielding the following relationship:

$$\delta^{18}O = (-4.02\times10^{-7} \pm 1.26\times10^{-7})h^2 + -(0.0012 \pm 0.0005)h - (8.02 \pm 0.46) \qquad (2)$$

Sample 99kg23 has been omitted from the regression because it is clearly anomalous, and it significantly modifies the best-fit curve. We choose a second order polynomial fit because it allows for variation from pure Rayleigh fractionation, present in the data, that can result from processes such as evapotranspiration and mixing of vapor masses.

Two minor rainfall events occurred in the late afternoon between Larjung and Beni (Fig. 5). On both afternoons, drizzle fell over a 2–3 h period and stream discharge increased. Little scatter in the data between Larjung and Beni indicates that these events did not significantly modify tributary $\delta^{18}O$ values. This suggests that tributary discharge during the months after the monsoon season is dominated by groundwater discharge of monsoon rainfall.

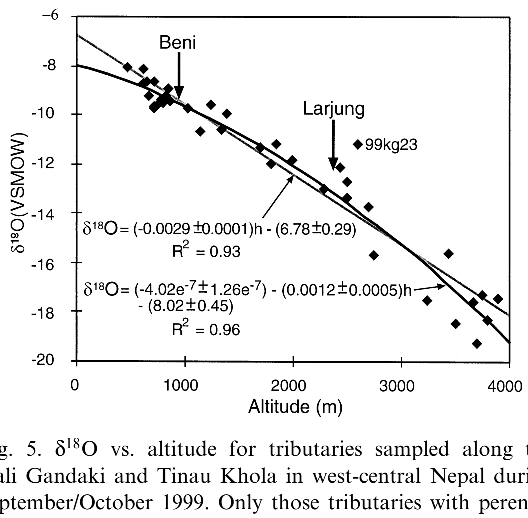

Fig. 5. $\delta^{18}O$ vs. altitude for tributaries sampled along the Kali Gandaki and Tinau Khola in west-central Nepal during September/October 1999. Only those tributaries with perennial flow over an elevation range of <2000 m are plotted in the arid region north of the high Himalaya. Line fit is shown in gray, and second order polynomial fit in black.

6. Discussion

6.1. Mean rainfall elevation in tributary drainage basins

Tributaries carry meteoric water that fell over a range of elevations in the drainage basin. The elevation of sampling is lower than the average elevation of the drainage basin and $\delta^{18}O$ values therefore reflect higher elevation rainfall than the rainfall at the elevation of sampling. For this reason, the *y*-intercept of the Kali Gandaki regression (−8‰) is more negative than the $\delta^{18}O$ value of mean annual precipitation in the modern Himalayan foreland (Fig. 5). We assume that the $\delta^{18}O$ value at New Delhi (elevation = 212 m, $\delta^{18}O = -5.81$, weighted mean [53]) is a representative value of precipitation in the foreland source region. We can estimate and correct for the difference between sampling elevation and the average elevation of the drainage basin by determining the difference in elevation that yields a curve that fits both New Delhi rainfall and $\delta^{18}O$ values of Kali Gandaki tributaries (Fig. 6). At an elevation difference of 1000 m, the best-fit polynomial has a *y*-intercept of −6.0‰, approaching the value for New Delhi rainfall. Above 1000 m there is no significant change in the *y*-intercept of the best-fit second order polynomial. An elevation difference of 1000 m between sampling elevation and average elevation of the drainage basin seems reasonable given that the streams we sampled source water over a range of elevations from 160 to 2300 m above the sampling elevation (Table 1). The second order polynomial that fits New Delhi precipitation and defines a 1000 m elevation difference above the sampling elevations is defined by:

$$\delta^{18}O = (-2.61\times10^{-7} \pm 0.84\times10^{-7})h^2 + (-0.0013 \pm 0.0005)h - (6.00 \pm 0.69) \quad (3)$$

(termed 'Kali Gandaki relationship'). Tributaries of the Seti River fall within the range of scatter of the Kali Gandaki data, assuming an average elevation of rainfall 600 m above the sampling elevation (Fig. 7). The difference in the apparent average elevation of rainfall probably resulted from a greater proportion of more positive winter/spring rainfall in Seti River tributaries because there were anomalously large rainfall events during our sampling. However this is difficult to resolve because the sample set is small and represents a narrow range of elevations.

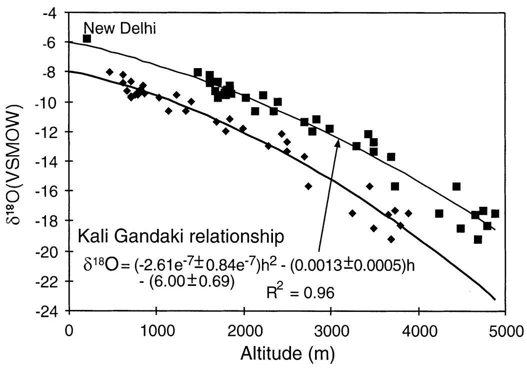

Fig. 6. $\delta^{18}O$ vs. altitude for Kali Gandaki tributaries corrected for the difference between sampling elevation and average rainfall elevation. Diamonds show $\delta^{18}O$ values of tributaries at the sampling elevation. Note the *y*-value at 200 m (approximate elevation of the Gangetic foreland) does not equal the average annual rainfall at New Delhi ($\delta^{18}O = -5.81$‰, weighted mean [53]) in the foreland. Squares show $\delta^{18}O$ values of tributaries at 1000 m higher than the sampling elevation. The best-fit second order polynomial to both the New Delhi value and elevation-corrected data is shown. See text for discussion.

6.2. $\delta^{18}O$ vs. altitude relationship

The Kali Gandaki transect provides the best constraints on the regional $\delta^{18}O_{mw}$ vs. altitude relationship because it covers the largest range of elevations, and tributary $\delta^{18}O$ values did not experience perturbations from rainfall events. Rainout by a Rayleigh fractionation process predicts that $\delta^{18}O_{mw}$ will become increasingly more negative with each rainout event. The second order polynomial fit to the $\delta^{18}O_{mw}$ vs. altitude relationship for Kali Gandaki tributaries displays this depletion and is consistent with a Rayleigh-type fractionation process. Rowley and Pierrehumbert used atmospheric thermodynamic relations, based on relative humidity and temperature, in a Rayleigh-type fractionation model to predict the oxygen isotopic composition of rainfall with increas-

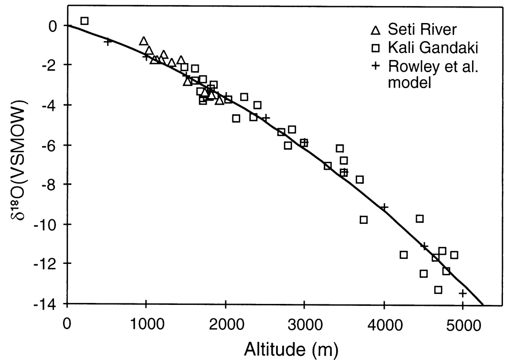

Fig. 7. The Kali Gandaki relationship (black line) compared to the $\delta^{18}O$/altitude model of Rowley and Pierrehumbert [54] (crosses) and elevation-corrected data from the Kali Gandaki and Seti River transects. See text for discussion.

ing elevation in the tropics [54]. Data presented here provide an empirical relationship that can be compared with the model of Rowley and Pierrehumbert. By setting the y-intercept to 0‰, the Kali Gandaki relationship can be compared to their model or any region with different source moisture values (Fig. 7). The agreement between our data and the model of Rowley and Pierrehumbert is striking.

All of the small tributaries we sampled along the Kali Gandaki (except 99kg23) fall within ±1.5‰ of the Kali Gandaki relationship (Fig. 7). We therefore take ±1.5‰ as the range of error in the y-axis of the relationship. This yields errors in elevation estimates of less than ±560 m for regions over 3000 m.

6.3. Modern meteoric water vs. the carbonate record

The modern $\delta^{18}O_{mw}$ vs. altitude relationship can be used to reconstruct the paleoelevation during carbonate formation. A variety of factors influence the $\delta^{18}O$ values of carbonate, such as the $\delta^{18}O_{mw}$, evaporation, diagenetic effects, and temperature of calcite/aragonite precipitation. Diagenetic processes can be gauged independently through petrographic observations and by analyzing diagenetic carbonate to determine the isotopic composition of diagenetic fluids. The degree of fractionation as a result of evaporation is difficult to quantify. In lacustrine carbonate deposits relative changes in evaporation can be assessed using changes in Mg/Ca ratios and by comparing percent aragonite to percent calcite. Comparing different types of carbonate can help in determining whether one type has been enriched in ^{18}O by evaporation or other processes.

Oxygen isotopic fractionation between calcite and water (α_{c-w}) depends on the temperature of calcite precipitation:

$$1000\ln\alpha_{c-w} = 2.78(10^6 T^{-2}) - 2.89 \quad (4)$$

where the fractionation factor $\alpha_{c-w} = (^{18}O/^{16}O)_c/(^{18}O/^{16}O)_w$ and T is absolute temperature [55]. Assumptions must be made about average annual temperature and the season of carbonate precipitation in order to use this equation to calculate $\delta^{18}O_{mw}$. An uncertainty of ±10°C only introduces an error of ±2.3‰ to the $\delta^{18}O_{mw}$ estimate[1], which is minor compared to the degree of fractionation associated with changes in elevation.

Garzione et al. [11] inferred that the Thakkhola graben in the southern Tibetan Plateau has been at an elevation similar to modern since the onset of deposition in the graben, based on very low $\delta^{18}O_c$ values from lacustrine and paleosol carbonate in the Late Miocene–Pliocene basin fill (data available in **EPSL Online Background Dataset**[2])[11]. A range of paleoelevations can be estimated from these carbonates using the Kali Gandaki relationship. Today the average annual temperature of Lo Manthang, in northern Thakkhola graben is 6°C[3] (3750 m above sea level) [57]. In lacustrine systems, the average annual

[1] We use the equation of Friedman and O'Neil [55] instead of the more recently published equation by Kim and O'Neil [56] to better compare calculated meteoric water values to past studies that use the Friedman and O'Neil equation. Using the Kim and O'Neil equation would produce calculated meteoric water values up to 0.4‰ lower, which would increase paleoelevation estimates by up to ~100 m.

[2] http://www.elsevier.nl/locate/epsl, mirror site: http://www.elsevier.com/locate/epsl

[3] Mean of average monthly maximum and minimum temperatures from data available between 1974 and 1994.

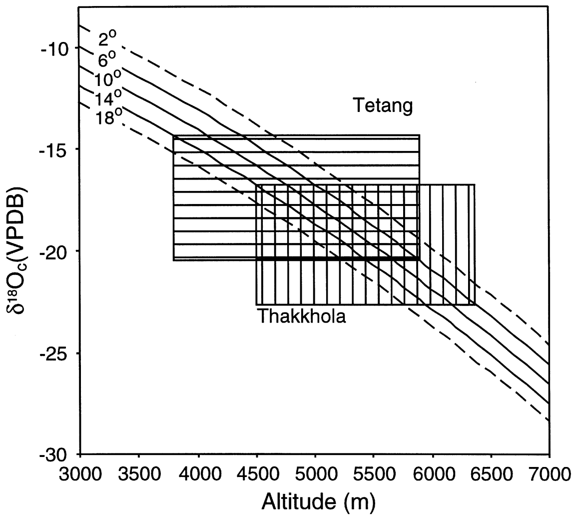

Fig. 8. $\delta^{18}O_c$ values calculated from the Kali Gandaki relationship for calcite that precipitated from water at temperatures between 2 and 18°C plotted against altitude. Solid lines show 6–14°C, which is the most reasonable range of temperatures for the precipitation of Thakkhola graben carbonates. Boxes show the range of elevations predicted from the range of $\delta^{18}O_c$ values of Thakkhola Formation carbonates (vertical lines) and Tetang Formation carbonates (horizontal lines). Tetang Formation $\delta^{18}O_c$ values have been shifted by 3‰ to reflect the difference in source moisture values prior to 7 Ma.

temperature is a reasonable minimum temperature for calcite precipitation because most lacustrine carbonate precipitates during the warm season when lakes are most productive. The average temperature for July (warmest month) in Lo Manthang is 14°C [57], which represents a reasonable maximum temperature for lake water and carbonate precipitation. Paleosol carbonate probably precipitated over a similar 6–14°C temperature range because soil carbonate is thought to form during the growing season as soil is dewatered by evapotranspiration [58]. Average monthly temperatures in Lo Manthang are between 6 and 14°C from April to October [57], and the assumption is that most lacustrine and paleosol carbonate precipitated during these months.

To incorporate the error associated with the temperature of calcite precipitation, we determined the $\delta^{18}O_c$ values from the Kali Gandaki relationship over the inferred range of temperatures of calcite precipitation in the Thakkhola graben (Fig. 8). The $\delta^{18}O_c$ values from the Thakkhola Formation (data available in **EPSL Online Background Dataset**[2]) are superimposed on this (vertical line pattern). Elevations of 4500 ± 430 m to 6300 ± 330 m are predicted by the Kali Gandaki relationship for calcite that precipitated at temperatures between 6 and 14°C. These elevations represent the source region of meteoric water in the basin and are in agreement with the elevations of the peaks surrounding the basin today (up to 6700 m).

Modern $\delta^{18}O_{mw}$ from the Thakkhola graben can be compared with predicted $\delta^{18}O_{mw}$ values from Thakkhola graben carbonate. It is likely that monsoon conditions have prevailed in southern Asia since at least 8 Ma during deposition of the Thakkhola Formation (< 7 Ma) [59,60]. In addition, the $\delta^{18}O_c$ values of paleosol carbonate from Siwalik foreland basin deposits do not change significantly over the last 7 Ma [61] and compare well with source moisture from the modern Himalayan foreland, indicating that the $\delta^{18}O$ value of source moisture has remained fairly constant. We compare both large and small tributaries in order to gauge the full range of water derived from basin floor precipitation to snow melt run-off from the peaks that flank the basin. The range of tributary $\delta^{18}O$ values is −15.7‰ to −21.2‰, from 2960 to 3900 m (Table 1). Kali Gandaki water sampled in September 1997 and 1999 (97kg1, 99kg3, and 99kg13) from two locations in the graben ranges from −18.2 to −19.5, which reflects the average of tributary $\delta^{18}O$ values. However, predicted $\delta^{18}O_{mw}$ values from carbonate of the Thakkhola Formation range from −17.8‰ to −23.2‰ (calculated at 12°C), which is ~2‰ more negative than modern $\delta^{18}O_{mw}$ values. This difference can be explained by changes in local elevation. We sampled tributary water within the Kali Gandaki gorge (average sampling elevation = 3480 m), which has incised the Thakkhola graben fill by ~1000 m. Assuming the basin floor elevation was approximately 4000 m during deposition of the Thakkhola Formation, the elevation difference accounts for ~1.7‰ of the 2‰ increase in modern meteoric water. Therefore modern $\delta^{18}O_{mw}$ values agree very well with meteoric water values predicted from Thakkhola graben carbonate.

Additional climatic variables must be taken into consideration in determining paleoelevation from Tetang Formation carbonate (data available in **EPSL Online Background Dataset**[2]). Several lines of evidence suggest that the regional weather patterns may have been different [2,59–61] prior to 8 Ma. In addition, the $\delta^{18}O$ values of soil carbonate from the Siwalik Group display an ~3‰ increase at ~7 Ma, suggesting that source moisture traveling northward from the foreland basin could have been as much as 3‰ more negative prior to 7 Ma [61]. Dettman et al. documented strong seasonal variations in oxygen isotopes of fossil mollusks from the Siwalik Group (back to ~10.7 Ma), similar to variations observed under modern monsoon conditions [62]. They inferred that the monsoon existed prior to 7.5 Ma, but that monsoon rainout was more intense and the dry season was less dry. Under these conditions, the ~3‰ increase in the soil carbonate record at ~7 Ma would have resulted from higher $\delta^{18}O$ values of monsoon rainfall (from less intense rainout) and more evaporation from soils during the more arid dry season. In the simplest case, we assume that the $\delta^{18}O_{mw}$ vs. altitude gradient was the same as the modern gradient and that source moisture (at ~200 m elevation) was 3‰ lower during Tetang deposition. In Fig. 8 the $\delta^{18}O_c$ values of Tetang Formation carbonate (−17.2‰ to −23.4‰) are shifted by 3‰ to account for different source moisture values prior to 7 Ma. Elevations of the source regions of meteoric water are estimated to be 3800±480 m to 5900±350 m for calcite that precipitated at temperatures between 6 and 14°C. Absolute paleoelevation estimates for the Tetang Formation are 400 m to 700 m lower than those predicted for the Thakkhola Formation, but agree within error. High elevation during the late Miocene is consistent with observations from the Himalayan fold–thrust belt, which indicate that the region south of the Indus Suture Zone had experienced major crustal thickening by Oligocene time.

Two significant unknowns that introduce error into the paleoelevation estimates are the degree of evaporative enrichment of ^{18}O in paleometeoric water and the paleotemperature of calcite precipitation. These two variables offset each other. Assuming some degree of evaporative enrichment would increase the paleoelevation estimate, whereas a higher temperature of calcite precipitation as a result of warmer temperatures in the Miocene would decrease the estimate. Oxygen isotopic data of planktonic foraminifera from the late Miocene suggest that equatorial sea surface temperatures were similar to Holocene sea surface temperatures [63], which may indicate that equatorial continental temperatures were similar to today. Even if calcite precipitation occurred at temperatures of 10°C warmer, the paleoelevation estimates would only be reduced by ~500–600 m. The role of evaporation cannot be discounted and may cause an underestimation of paleoelevation.

7. Conclusions

Values of $\delta^{18}O_c$ of paleocarbonate can provide useful insights into paleoelevation, where supported by an understanding of the modern variation in $\delta^{18}O_{mw}$ with altitude. This study determines an empirical relationship for the modern $\delta^{18}O_{mw}$ vs. altitude gradient across the Himalaya by analyzing water from small tributaries across two thrust belt transects. A second order polynomial (Eq. 2) provides the best fit to $\delta^{18}O$ values of tributary water sampled over a 3200 m range of elevations along the Kali Gandaki in west-central Nepal. An elevation correction that fits both average annual meteoric water at New Delhi and the $\delta^{18}O$ values of Kali Gandaki tributaries suggests that rainfall in the tributary basins occurs on average 1000 m higher than the sampling elevation. This elevation-corrected equation is termed the 'Kali Gandaki relationship' (Eq. 3) and is used to estimate the paleoelevation of the Thakkhola graben from carbonate deposited in the graben.

Very negative $\delta^{18}O_{mw}$ values inferred from carbonate of the Thakkhola graben on the southern edge of the Tibetan Plateau suggest that this region has been at a high elevation since the onset of deposition in the basin between 10.5 and 11

Ma. Elevations of 4500 ± 430 m to 6300 ± 330 m are predicted by the Kali Gandaki relationship for Thakkhola Formation carbonate. Carbonate of the Tetang Formation produces paleoelevation estimates between 3800 ± 480 m to 5900 ± 350 m. Tetang and Thakkhola formation paleoelevation estimates are within error of each other and are similar to modern elevations on the Tibetan Plateau. High elevation since the onset of deposition in the Thakkhola graben is consistent with data on the kinematic and metamorphic history of the Himalayan fold–thrust belt, which suggest significant elevations were attained by Oligocene time.

Acknowledgements

We thank D. Hodkinson, D. Robinson, B. Upreti, B. LaReau, T. Ojha, and P. Kaminski for their enthusiastic assistance in the field. Thanks also go to D. Dettman for valuable discussions and comments on an early version of the manuscript and for assistance in the lab. The manuscript was improved by reviews from C. Drummond and B. Wilkinson. This project was supported by donors to the Geostructure Industrial Partnership at the University of Arizona, NSF Grant EAR-9725607 (to DeCelles and Quade), and the Institute for the Study of Planet Earth at the University of Arizona.*[RV]*

References

[1] E.J. Fielding, B.L. Isacks, M. Barazangi, C. Duncan, How flat is Tibet?, Geology 22 (1994) 163–167.
[2] J. Quade, T.E. Cerling, J.R. Bowman, Development of Asian monsoon revealed by marked ecological shift during the latest Miocene in northern Pakistan, Nature 342 (1989) 163–166.
[3] M.E. Raymo, W.F. Ruddiman, Tectonic forcing of late Cenozoic climate, Nature 359 (1992) 117–122.
[4] J.M. Edmond, Himalayan tectonics, weathering processes, and the strontium isotopic record in marine limestones, Science 258 (1992) 1594–1597.
[5] W.L. Prell, J.E. Kutzbach, Sensitivity of the Indian monsoon to forcing parameters and implications for its evolution, Nature 360 (1992) 647–652.
[6] T.M. Harrison, P. Copeland, W.F.S. Kidd, A. Yin, Raising Tibet, Science 255 (1992) 1663–1670.
[7] P. Molnar, P. England, J. Martinod, Mantle dynamics, uplift of the Tibetan Plateau, and the Indian monsoon, Rev. Geophys. 31 (1993) 357–396.
[8] L.A. Derry, C. France-Lanord, Neogene Himilayan weathering history and river $^{87}Sr/^{86}Sr$: Impact on the marine Sr record, Earth Planet. Sci. Lett. 142 (1996) 59–74.
[9] C.N. Drummond, B.H. Wilkinson, K.C. Lohmann, G.R. Smith, Effect of regional topography and hydrology on the lacustrine isotopic record of Miocene paleoclimate in the Rocky Mountains, Palaeogeogr. Palaeoclimatol. Palaeoecol. 101 (1993) 67–79.
[10] D.L. Dettman, K.C. Lohmann, Oxygen isotope evidence for high-altitude snow in the Laramide Rocky Mountains of north America during the Late Cretaceous and Paleogene, Geology 28 (2000) 243–246.
[11] C.N. Garzione, D.L. Dettman, J. Quade, P.G. DeCelles, R.F. Butler, High times on the Tibetan Plateau: paleoelevation of the Thakkhola graben, Nepal, Geology 28 (2000) 339–342.
[12] M.A. Poage, C.P. Chamberlain, Empirial relationship between elevation and the stable isotope composition of precipitation: considerations for studies of paleoelevation change, Am. J. Sci., in review.
[13] U. Dansgaard, Stable isotopes in precipitation, Tellus 16 (1964) 436–468.
[14] U. Siegenthaler, H. Oeschger, Correlation of ^{18}O in precipitation with temperature and altitude, Nature 285 (1980) 314–317.
[15] K. Rozanski, C. Sonntag, Vertical distribution of deuterium in atmospheric water vapour, Tellus 34 (1982) 135–141.
[16] N.L. Ingraham, B.E. Taylor, Hydrogen isotope study of large-scale meteoric water transport in northern California and Nevada, J. Hydrol. 85 (1986) 183–197.
[17] R. Ramesh, M.M. Sarin, Stable istope study of the Ganga (Ganges) river system, J. Hydrol. 139 (1992) 49–62.
[18] S.K. Bartarya, S.K. Bhattacharya, R. Ramesh, B.L.K. Somayajulu, $\delta^{18}O$ and δD systematics in the surficial waters of the Gaula river catchment area, Kumaun Himalaya, India, J. Hydrol. 167 (1995) 369–379.
[19] J. Grabczak, M. Kotarba, Isotopic composition of the thermal waters in the central part of the Nepal Himalayas, Geothermics 14 (1985) 567–575.
[20] P. Fritz, River waters, in: J.R. Gat, R. Gonfiatini (Eds.), Stable Isotope Hydrology: D and ^{18}O in the Water Cycle, IAEA, Vienna, Techn. Rep. Ser., no. 210 (1981) 177–199.
[21] C.J. Yonge, L. Goldenberg, H.R. Krouse, An isotopic study of water bodies along a traverse of southwestern Canada, J. Hydrol. 106 (1989) 245–255.
[22] A. Gansser, Geology of the Himalayas, Interscience, London, 1964, 289 pp.
[23] M.P. Searle, Structural evolution and sequence of thrusting in the high Himalaya, Tibetan Tethys and Indus suture zones of Zanskar and Ladakh, western Himalaya, J. Struct. Geol. 8 (1986) 923–936.
[24] J.P. Burg, G.M. Chen, Tectonics and structural zonation of southern Tibet, China, Nature 311 (1984) 219–223.

[25] L. Ratschbacher, W. Frisch, L. Guanghua, C. Chengsheng, Distributed deformation in southern and western Tibet during and after the India–Asia collision, J. Geophys. Res. 99 (1994) 19917–19945.

[26] B.C. Burchfiel, C. Zhiliang, K.V. Hodges, L. Yuping, L.H. Royden, D. Changrong, X. Jiene, The south Tibetan detachment system, Himalayan orogen: extension contemporaneous with and parallel to shortening in a collisional mountain belt, GSA Spec. Pap. 269, 1992, 41 pp.

[27] R.R. Parrish, K.V. Hodges, Isotopic constraints on the age and provenance of the Lesser and Greater Himalayan sequences, Nepalese Himalaya, Geol. Soc. Am. Bull. 108 (1996) 904–911.

[28] P.G. DeCelles, G.E. Gehrels, J. Quade, B. LaReau, M. Spurlin, Tectonic implications of U-Pb zircon ages of the Himalayan Orogenic belt in Nepal, Science 288 (2000) 497–499.

[29] K.S. Valdiya, Geology of the Kumaon Lesser Himalaya, Wadia Institute of Himalayan Geology, 1980, 291 pp.

[30] J. Stöcklin, Geology of Nepal and its regional frame, Geol. Soc. Lond. J. 137 (1980) 1–34.

[31] D. Schelling, The tectonostratigraphy and structure of the eastern Nepal Himalaya, Tectonics 11 (1992) 925–943.

[32] P. Srivastava, G. Mitra, Thrust geometries and deep structure of the outer and lesser Himalaya, Kumaon and Garhwal (India): Implications for evolution of the Himalayan fold–thrust belt, Tectonics 13 (1994) 89–109.

[33] P.G. DeCelles, G.E. Gehrels, J. Quade, T.P. Ojha, Eocene–early Miocene foreland basin development and the history of Himalayan thrusting, western and central Nepal, Tectonics 17 (1998) 741–765.

[34] K.V. Hodges, D.S. Silverburg, Thermal evolution of the greater Himalaya, Garhwal, India, Tectonics 7 (1988) 583–600.

[35] M.S. Hubbard, T.M. Harrison, $^{40}Ar/^{39}Ar$ age constraints of deformation and metamorphism in the Main Central thrust zone and Tibetan slab, eastern Nepal Himalaya, Tectonics 8 (1989) 865–880.

[36] K.V. Hodges, R.R. Parrish, M.P. Searle, Tectonic evolution of the central Annapurna range, Nepalese Himalayas, Tectonics 15 (1996) 1264–1291.

[37] M.E. Coleman, U–Pb constraints on Oligocene–Miocene deformation and anatexis, Marsyangdi Valley, central Nepalese Himalaya, Am. J. Sci. 298 (1998) 553–571.

[38] J.L. Mugnier, G. Mascle, T. Faucher, Structure of the Siwaliks of western Nepal: an intracontinental accretionary prism, Int. Geol. Rev. 35 (1993) 32–47.

[39] P.G. DeCelles, G.E. Gehrels, J. Quade, T.P. Ojha, P.A. Kapp, B.N. Upreti, Neogene foreland basin deposits, erosional unroofing, and kinematic history of the Himalayan fold–thrust belt, western Nepal, Geol. Soc. Am. Bull. 110 (1998) 2–21.

[40] H. Lyon-Caen, P. Molnar, Gravity anomalies, flexure of the Indian plate, and the structure, support and evolution of the Himalaya and Ganga basin, Tectonics 4 (1985) 513–538.

[41] P.M. Powers, R.J. Lillie, R.S. Yeates, Structure and shortening of the Kangra and Dehra Dun reentrants, sub-Himalaya, India, Geol. Soc. Am. Bull. 110 (1998) 1010–1027.

[42] R. Bilham, K. Larson, J. Freymuller, Indo–Asian convergence rates in the Nepal Himalaya, Nature 386 (1997) 61–64.

[43] Y.M.R. Najman, M.S. Pringle, M.R.W. Johnson, A.H.F. Robertson, J.R. Wijbras, Laser ^{40}Ar–^{39}Ar dating of single detrital muscovite grains from early foreland-basin sedimentary deposits in India: Implications for early Himalayan evolution, Geology 25 (1997) 535–538.

[44] M. Colchen, P. LeFort, A., Pêcher, 1986. Annapurna–Manaslu–Ganesh Himal notice de la carte geologique au 1/200000, Centre Natl. Rech. Sci., Paris, 1986, 136 pp.

[45] M. Fort, P. Freytet, M. Colchen, Structural and sedimentological evolution of the Thakkhola Mustang graben (Nepal Himalayas), Z. Geomorphol. 42 (1982) 75–98.

[46] C.N. Garzione, Tectonic and paleoelevation history of the Thakkhola graben and implications for the evolution of the southern Tibetan Plateau, Ph.D. Thesis, Tucson, AZ, 2000, 146 pp.

[47] S. Iwata, Geomorphology of the Thakkhola–Muktinath region, central Nepal, and its Late Quaternary history, Geogr. Rep. Tokyo Metrol. Univ. 19 (1984) 25–42.

[48] J.M. Hurtado, K.V. Hodges, K.X. Whipple, Neotectonics of the Thakkhola graben and implications for recent activity on the South Tibetan fault system in the central Nepalese Himalaya. Geol. Soc. Am. Bull., in press.

[49] NOAA, global historical climatology network (www.ncdc.noaa.gov).

[50] S.R. Chalise, M.L. Shrestha, K.B. Thapa, B.R. Shrestha, and B. Bajracharya, Climatic and hydrological Atlas of Nepal, International Centre for Integrated Mountain Development, Kathmandu, Nepal, 1996, 264 pp.

[51] J.-E. Hurtrez, Analyse géomorphologique des interactions Tectonique-Erosion dans le systéme Himalayan. Ph.D. Thesis, Montpellier, 1998.

[52] N.B. English, J. Quade, P.G. DeCelles, C.N. Garzione, Geologic control of Sr and major element chemistry in Himalayan reivers, Nepal, Geochim. Cosmochim. Acta 64 (2000) 2549–2566.

[53] K. Rozanski, L. Araguás-Arguás, r. Gonfiantini, Isotopic patterns in modern global precipitation, in: P. Swart, J.A. McKenzie, K.C. Lohmann, (Eds.), Continental Indicators of Climate, Proceedings of the Chapman Conference, Jackson Hole, WY. Am. Geophys. Union Monograph 78 (1993) 1–36.

[54] D.B. Rowley, R.T. Pierrehumbert, Stable isotope-based paleoaltimetry, Earth. Planet. Sci. Lett., in review.

[55] I. Friedman, J.R. O'Neil, Compilation of stable isotope fractionation factors of geochemical interest, in: M. Fleischer (Ed.), Data of Geochemistry, Chapter KK: US Geological Survey Professional Paper 440-K, 1977, 12 pp.

[56] S.T. Kim, J.R. O'Neil, Equilibrium and nonequilibrium oxygen isotope effects in synthetic carbonates, Geochim. Cosmochim. Acta 61 (1997) 3461–3475.

[57] Department of Hydrology and Meteorology, Precipitation Records of Nepal, 1974–1994, His Majesty's Government of Nepal, Ministry of Water Resources, Department of Hydrology and Meteorology, Kathmandu, Nepal, 1996.

[58] T.E. Cerling, Y. Wang, Stable carbon and oxygen isotopes in soil CO_2 and soil carbonates: Theory, practice, and application to some prairie soils of upper Midwestern North America, in: T.W. Boutton, S. Yamasaki (Eds.), Mass Spectrometry of Soils, Marcel Dekker, New York, 1996, pp. 113–131.

[59] D. Kroon, T. Steens, S.R. Troelstra, Onset of monsoonal related uplift in the western Arabian sea as revealed by planktonic foraminifera, Proc. Ocean Drill. Progr. Sci. Results 117 (1991) 257–263.

[60] W.L. Prell, D.W. Murray, S.C. Clemens, D.M. Anderson, Evolution and variability of the Indian Ocean summer monsoon: Evidence from the western Arabian Sea drilling program, in: R.A. Duncan et al., (Eds.), Synthesis of Results from Scientific Drilling in the Indian Ocean, Geophys. Monogr. Ser. 70 (1992) 447–469.

[61] J. Quade, J.M.L. Cater, T.P. Ojha, J. Adam, T.M. Harrison, Late miocene environmental change in Nepal and the northern Indian subcontinent: Stable isotopic evidence from paleosols, Geol. Soc. Am. Bull. 107 (1995) 1381–1397.

[62] D.L. Dettman, M.J. Kohn, J. Quade, F.J. Ryerson, T.P. Ojha, S. Hamidullah, Seasonal stable isotope evidence for a strong Asian Monsoon throughout the last 10.7 Ma, Geology, in review.

[63] S.M. Savin, D. Hodell, J.P. Kennett, M. Murphy, G. Keller, J. Killingley, E. Vincent, The evolution of Miocene surface and near-surface marine temperatures: Oxygen isotopic evidence, Geol. Soc. Am. Memoir 163 (1985) 49–73.